Electronic Supplementary Material (ESI) for Materials Chemistry Frontiers.

Supporting Information

Hierarchical porous N-doped carbon electrode with superior rate performance and cyclic stability for flexible supercapacitors

Meng Cheng,[ab] Yuena Meng,*[a] Qinghai Meng,[b] Lijuan Mao,[b] Miao Zhang,[b] Kamran Amin,[b] Aziz Ahmad,[b] Sixin Wu*[a] and Zhixiang Wei*[b]

a. The Key Laboratory for Special Functional Material, Henan University, Kaifeng, 474004, P. R. China;

b. National Center for Nanoscience and Technology, No.11 Beiyitiao Zhongguancun Beijing 100190, P. R. China.

E-mail: weizx@nanoctr.cn; mengyuena@henu.edu.cn; wusixin@henu.edu.cn.

1. Synthesis graphite oxide

Graphite oxide (GO) was prepared from natural graphite by the method as follows: 2 g natural graphite powder and 1 g sodium nitrate ($NaNO_3$) were added to 46 mL concentrated sulfuric acid (H_2SO_4) solution in an ice bath. After 30 min of stirring, 6g potassium permanganate ($KMnO_4$) was added gradually while stirring for 2h. The suspended solution was then stirred at 35 °C for 1 h and carefully diluted with distilled water (92 mL) and the temperature of the reaction was increased to 98 °C for 1 h. After that, H_2O_2 (30%, 15 mL) was subsequently added to reduce the residual oxidant. Finally, the resulting brilliant-yellow mixture was left to stand overnight, after which the solid matter was washed with HCl aqueous solution (1:10) to remove the metal ions and then washed repeatedly with H_2O to neutralize by centrifugation. The solid obtained was dried under vacuum, and graphite oxide was obtained. Based on the X-Ray Diffraction spectra (XRD, Figure S1) and Bragg equation, the layer spacing of the prepared graphite oxide is 0.72 nm.

Bragg equation: $2d\sin\theta = n\lambda$

Where λ is the wavelength of the X-rays, d is lattice plane spacing, n is the series of diffraction, θ is the angle between incident X-ray and corresponding crystal face.

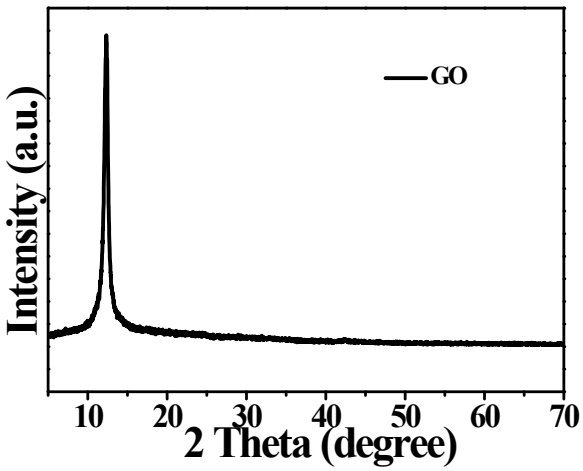

Figure S1. XRD pattern of obtained graphene oxide

2. Morphologies of RGO/NCs.

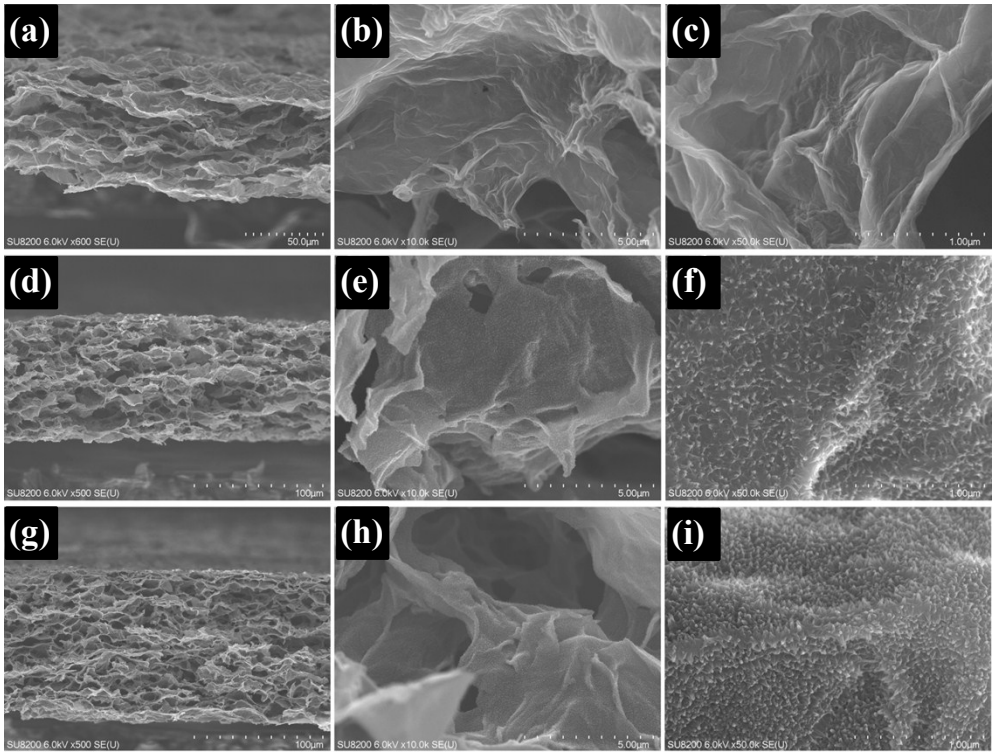

Figure S2. SEM images of (a,b,c) RGO/NC-1; (d,e,f) RGO/NC-2 and (g,h,i) RGO/NC-3.

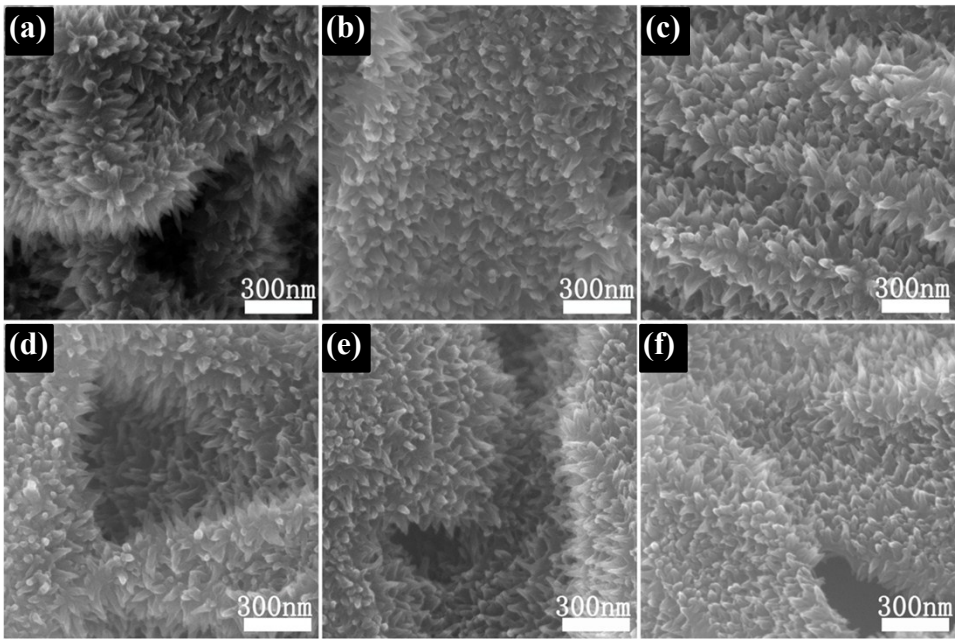

Figure S3. SEM images of the different reaction periods during three-step carbonization. (a) - (f) corresponding to I, II, III, IV, V, and VI.

3. Characterization

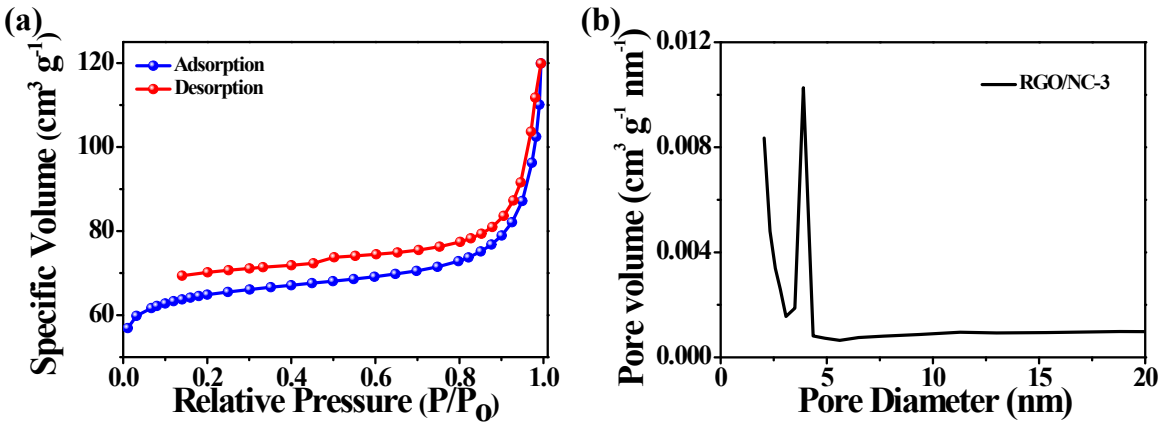

Figure S4. N2 adsorption/desorption isotherms at 77 K (a) and the pore size distribution curves (b) of three-dimensional RGO/NC-3.

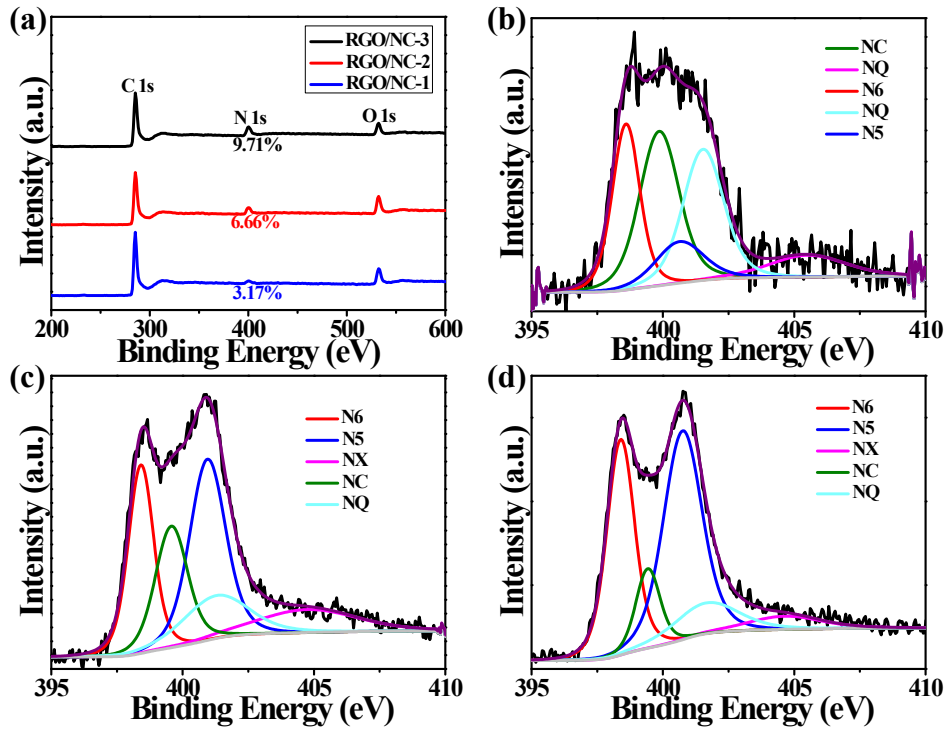

Figure S5. Wide-scan XPS spectra of RGO/NCs (a); and fitted high-resolution XPS spectra of N 1s of RGO/NC-1 (b); RGO/NC-2 (c); and 3DRGO/NC-3 (d).

Table S1. The elemental compositions of RGO/NCs and relative content of nitrogen species in these samples.

Samples	C (%)	N (%)	O (%)	N6 (%)	NC (%)	N5 (%)	NQ (%)	NX (%)
RGO/NC-1	87.87	3.17	8.97	0.74	0.98	0.32	0.86	0.27
RGO/NC-2	83.10	6.66	10.24	1.57	1.29	2.13	0.92	0.75
RGO/NC-3	83.74	9.71	6.55	3.06	0.99	4.13	1.04	0.49

The high-resolution XPS spectra of N 1s were measured to determine the state of doped nitrogen atoms, as shown in Figure S5 b-d. The N 1s spectra can be fitted into five peaks,

reflecting pyridinic-N (N6, 398.5 ± 0.1 eV), amides/amines or nitrile N (NC, 399.6 ± 0.2 eV), pyrrolic-N (N5, 400.7 ± 0.1 eV), quaternary-N (NQ, 401.7 ± 0.2 eV), and N-oxides (NX, 404-406 eV).[1-2] RGO/NC-3 contains more N6, N5 and NQ, NQ improves the conductivity, and N6 and N5 is the main contributor to pseudocapacitance.

Table S2. The assignment of the characteristic Raman peaks for three-dimensional RGO/PANI.

Raman bands (cm^{-1})	Assignment
1618	C–C stretching vibrations of the aromatic ring
1590	C-C stretching vibrations of the quinonoid ring
1513	N–H stretching vibration
1479	C=N stretching of quinoid rings
1414	phenazine-like or crosslinked structures
1336	$C–N^+$ vibration of delocalized polaronic structures
1239	C–N stretching vibration
1174	C–H bending vibration of benzenoid rings and quinoid rings

4. Electrochemical measurements

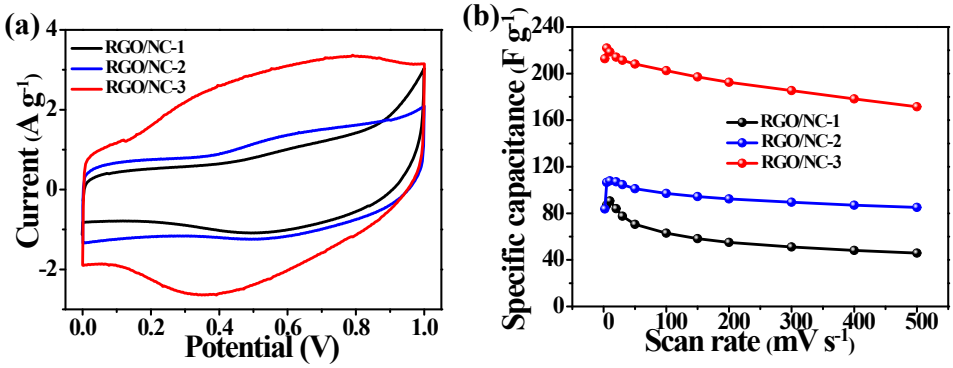

Figure S6. (a) Cyclic voltammetry curves of RGO/NC-1, RGO/NC-2 and RGO/NC-3 at a scan rate of 20 mV s^{-1}; (b) plot of specific capacitance calculated from CV curves at various scan rates.

The area of the curves is commonly used to calculate the value of the specific capacitance. The specific capacitance value of the three samples under scan rate varies from 2 mV s^{-1} to 500 mV s^{-1} have been represented in Figure S6b. Clearly, RGO/NC-3 reflects the highest specific capacitance among the three samples.

Table S3. Relative resistances of RGO/NCs samples obtained by fitting the EIS data.

Samples	R1	R2
RGO/NC-1	0.93	4.59
RGO/NC-2	0.92	1.33
RGO/NC-3	0.28	0.35

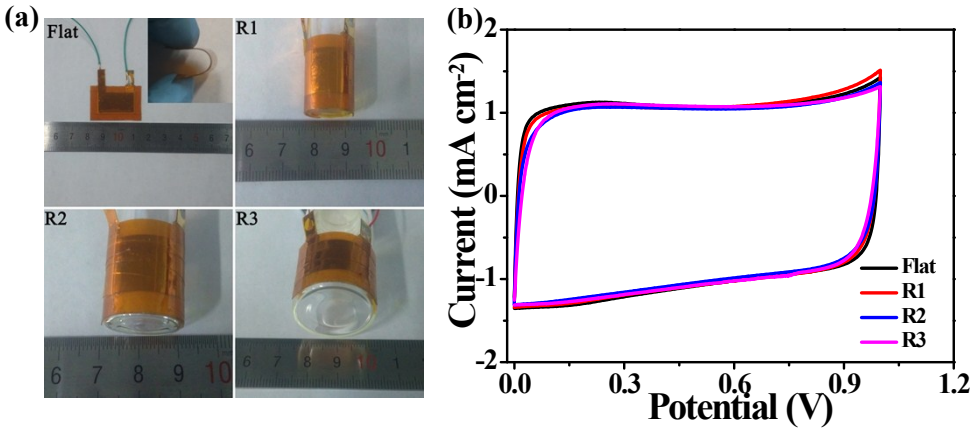

Figure S7. (a) Images of a flexible film supercapacitor bent into different states (R1=0.6 cm, R2=0.8 cm, R3=1.25 cm); (b) CV curves of the film supercapacitor at scan rate of 20 mV s^{-1} when in different bending states.

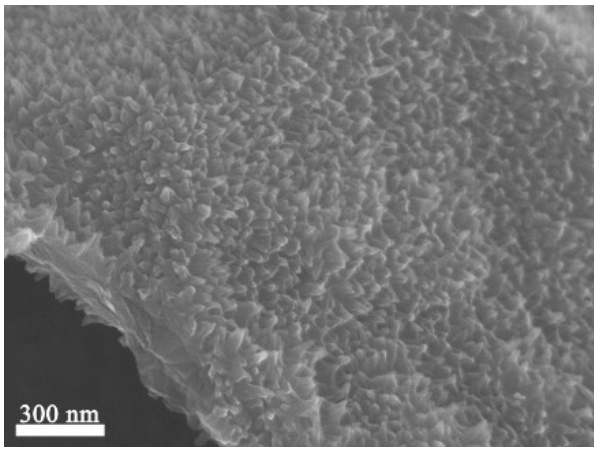

Figure S8. Morphology of electrode after GCD test.

Table S4. Energy density (E) and power density (P) of nitrogen-doped carbon for supercapacitors reported in our paper and other literatures

Materials	N content (wt%)	Electrolyte	Capacitance(F g^{-1})	E (W h kg^{-1})	P (W kg^{-1})	Ref
Porous NC	1.5	KOH	257 at 0.4 A g^{-1}; 204 at 10 A g^{-1}	7.25/5.43	/10000	[3]
NC nanofibrous	6.9	KOH	219 at 5 mV s^{-1}	5.8	19000	[4]
NC nanocage	10.9	KOH	313 at 1 A g^{-1}; 234 at 10 A g^{-1}	10.9/6.42	2500/22220	[5]
NCnanofiber	--	H_2SO_4	223.8 at 0.5 A g^{-1}; 175 at 10 A g^{-1}	5.9	1200	[6]
NC film	8.48	H_2SO_4	214 at 2 A g^{-1};	14.2	--	[7]
N-rich carbon	14.5	KOH	312 at 1 A g^{-1}; 115 at 100 A g^{-1}	9.2/0.11	4/23240	[8]
MWCNT/ZIF-8		H_2SO_4	112.4 at 0.5 A g^{-1}; 84.3 at 5 A g^{-1}	12.65/9.5	225.1/2257.2	[9]
Mesoporous NC	3.84	Na_2SO_4	148.1 at 0.5 A g^{-1};108 at 20 A g^{-1}	13.2/9.6	319.8/14400	[10]
N-doped graphene	6.85	H_2SO_4	242 at 1 A g^{-1};162 at 30 A g^{-1}	8.4/5.6	250/75000	[11]
Hierarchically NC	3.21	KOH	308.4 at 1 A g^{-1};258 at 10 A g^{-1}	10.7/9	500/5000	[12]
This work	**9.71**	**H_2SO_4**	**202 at 3A g^{-1}; 170 at 50 A g^{-1}**	**14/11.8**	**1500/25000**	

4. Bending test

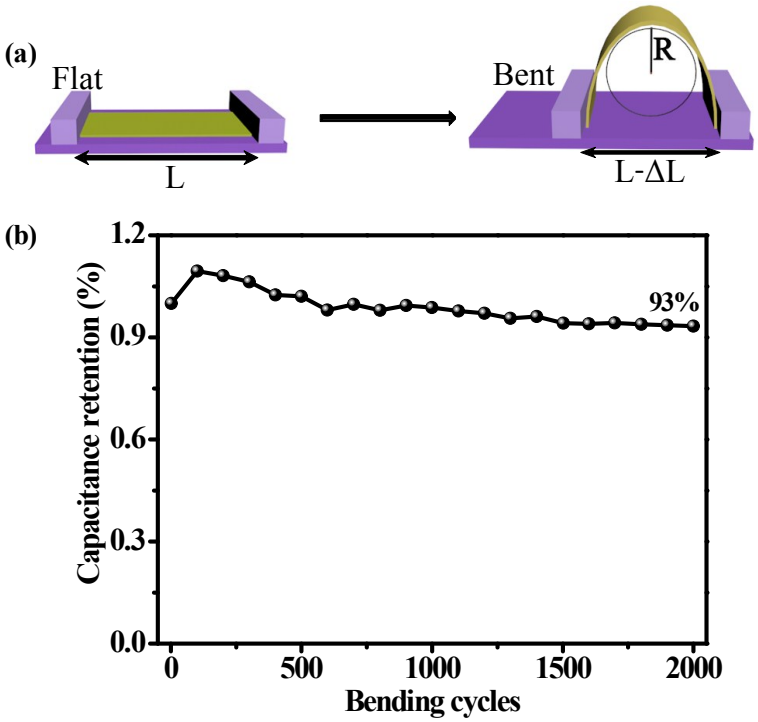

Figure S9. (a) Bending test of the three-dimensional RGO/NC-3 film supercapacitor on a bending stage device, (b) Capacitance retention of RGO/NC-3 film supercapacitor after 2000 cycles at 5 A g^{-1} during dynamic bending test.

The bend radius is given by[13]:

$$r = \frac{L}{2\pi\sqrt{\frac{\Delta L}{L} - \frac{\pi^2 h^2}{12L^2}}}$$

where L is initial length at flat state, (L-ΔL) is the length at bending state, and h is sample thickness. At the flat state, the length of the device is 3 cm (L). At the bending state, the distances (L-ΔL) are 2.5, 2, 1.5 and 1 cm corresponding to R1, R2, R3 and R4, respectively.

Therefore, the bending radii were 1.17, 0.83, 0.67 and 0.58 cm corresponding to R1, R2, R3 and R4, respectively.

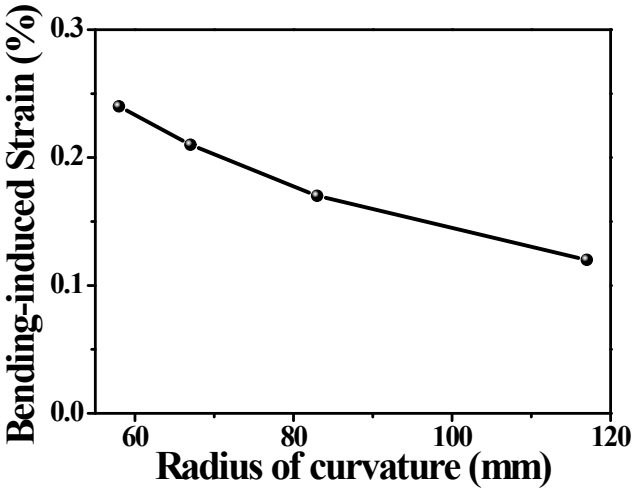

Figure S10. The bending-induced strain as a function of the radius of curvature.

The bending-induced strain was calculated using the following equation based on the following equation:

$$\varepsilon_{bending} = \frac{t_c}{2r_c}$$

where r_c is the radius of curvature, and t_c is the thickness of the flexible device (t_c is 0.28 mm).

5. Calculations

The power density and energy density were calculated using the following equations:

$$Ecell = \frac{1}{2}CV^2$$

$$Pcell = \frac{E}{t}$$

Where C is the specific capacitance of the coin-type cell, t is the discharge time (s).

Reference

S1 T. Palaniselvam, M. O. Valappil, R. Illathvalappil and S. Kurungot, *Energy Environ. Sci.*, 2014, **7**, 1059-1067.

S2 O. L. Li, S. Chiba, Y. Wada, G. Panomsuwan and T. Ishizaki, *J. Mater. Chem. A*, 2017, **DOI: 10.1039/C6TA08962C**.

S3 G. Wang, J. Zhang, S. Kuang, J. Zhou, W. Xing and S. Zhuo, *Electrochim. Acta*, 2015, **153**, 273-279.

S4 B. Duan, X. Gao, X. Yao, Y. Fang, L. Huang, J. Zhou and L. N. Zhang, *Nano Energy*, 2016, **27**, 482-491.

S5 J. Zhao, H. W. Lai, Z. Y. Lyu, Y. F. Jiang, K. Xie, X. Z. Wang, Q. Wu, L. J. Yang, Z. Jin, Y. W. Ma, J. Liu and Z. Hu, *Adv. Mater.*, 2015, **27**, 3541-3545.

S6 Y. L. Cheng, L. Huang, X. Xiao, B. Yao, L. Y. Yuan, T. Q. Li, Z. M. Hu, B. Wang, J. Wan and J. Zhou, *Nano Energy*, 2015, **15**, 66-74.

S7 Z. Li, L. Zhang, B. S. Amirkhiz, X. H. Tan, Z. W. Xu, H. L. Wang, B. C. Olsen, C. M. B. Holt and D. Mitlin, *Adv. Energy Mater.*, 2012, **2**, 431-437.

S8 F. Sun, J. Gao, X. Pi, L. Wang, Y. Yang, Z. Qu and S. Wu, *J. Power Sources*, 2017, **337**, 189-196.

S9 X. Li, C. Hao, B. Tang, Y. Wang, M. Liu, Y. Wang, Y. Zhu, C. Lu and Z. Tang, *Nanoscale*, 2017, **9**, 2178-2187.

S10 M. F. Chen, H. Q. Xuan, X. Z. Zheng, J. Y. Liu, X. P. Dong and F. N. Xi, *Electrochim. Acta*, 2017, **238**, 269-277.

S11 D. W. Wang, Y. G. Min, Y. H. Yu and B. Peng, *J. Colloid Interface Sci.*, 2014, **417**, 270-277.

S12 Q. Zhao, X. Wang, H. Xia, J. Liu, H. Wang, J. Gao, Y. Zhang, J. Liu, H. Zhou, X. Li, S. Zhang and X. Wang, *Electrochim. Acta*, 2015, **173**, 566-574.

S13 H. P. Wu, Q. H. Meng, Q. Yang, M. Zhang, K. Lu and Z. X. Wei, *Adv. Mater.*, 2015, **27**, 6504-6510.